

Extraordinary Transmission of Three-Dimensional Crescent-like Holes Arrays

Yang Shen · Mingkai Liu · Jensen Li · Xia Chen ·
Hai-Xia Xu · Qiangzhong Zhu · Xuehua Wang ·
Chongjun Jin

Received: 5 June 2011 / Accepted: 17 October 2011 / Published online: 22 November 2011
© The Author(s) 2011. This article is published with open access at Springerlink.com

Abstract We developed a method to fabricate a periodic array of three-dimensional crescent-like holes (3DCLH) via an inverted hemispherical colloidal lithography. It is found that there exists an extraordinary optical transmission in this non-planar perforated periodic array of 3DCLH when the electric field of the incident light is perpendicular to the cross-line of the crescent-like hole. This extraordinary optical peak is insensitive with the incident angles and sensitive with the angle between the electric field of the incident light to the cross-line of the 3DCLH. Numerical simulation based on finite-difference time-domain method reveals that this peak is caused by an asymmetric localized surface plasmon resonance. This structure might be useful for the optical sensing and optical-integrated circuits.

Keywords Surface plasmon polariton · Localized surface plasmon · Extraordinary optical transmission · Colloidal lithography

Introduction

Extraordinary optical transmission (EOT) of light passing through sub-wavelength holes array in a metallic film has

been found in 1998 [1]. It has attracted lots of attention, because this effect can be used in sub-wavelength integrated optical circuits [2–7], biosensors [8], surface plasmon enhanced Raman scattering [9, 10]. Lots of efforts have been made on this field in order to understand the fundamental physical mechanism and design more efficient structures [11–26]. Nowadays, it is considered that EOT of the sub-wavelength holes array is caused by the coupling between the incident waves and the surface plasmon polariton (SPP) with the help of the periodic two-dimensional holes array [7, 11]. In addition to circular holes arrays, EOT phenomenon was also found in holes arrays with different shapes, such as elliptical, rectangular, and annular holes [12–18]. Later, it is found that the localized surface plasmon resonance (LSP) could also play a role in the EOT in the holes with rectangular or elliptical shapes together with the SPP. To specify the contribution of the LSP, arrays of holes with a nanoparticle in each hole are fabricated and measured [19–22], it is found that both the SPP and the LSP contribute to the optical transmission, and both the real and imaginary parts of the polarizability of the particles which induce LSP play important roles in the transmission suppression and enhancement [20]. Very recently, an array of holes with very acute angles was found to exhibit a strong EOT effect caused by the LSP [27], an array of three-dimensional holes was also found that it has strong EOT effect induced by the LSP [28]. The waveguide mode across each hole can also play an important role in the extraordinary transmission through Fabry–Perot resonance [14, 29]. Until now, there have been no reports about the extraordinary transmission in a non-planar asymmetric structure. Here, we developed a unique fabrication method and prepared periodic arrays of three-dimensional crescent-like holes (3DCLH) as shown in Fig. 1a, by colloidal

Y. Shen · M. Liu · X. Chen · H.-X. Xu · Q. Zhu · X. Wang ·
C. Jin (✉)

State Key Laboratory of Optoelectronic Materials
and Technologies, School of Physics and Engineering,
Sun Yat-Sen University,
Guangzhou 510275, China
e-mail: jinchun@mail.sysu.edu.cn

J. Li
Department of Physics and Materials Science,
City University of Hong Kong,
Hong Kong, China

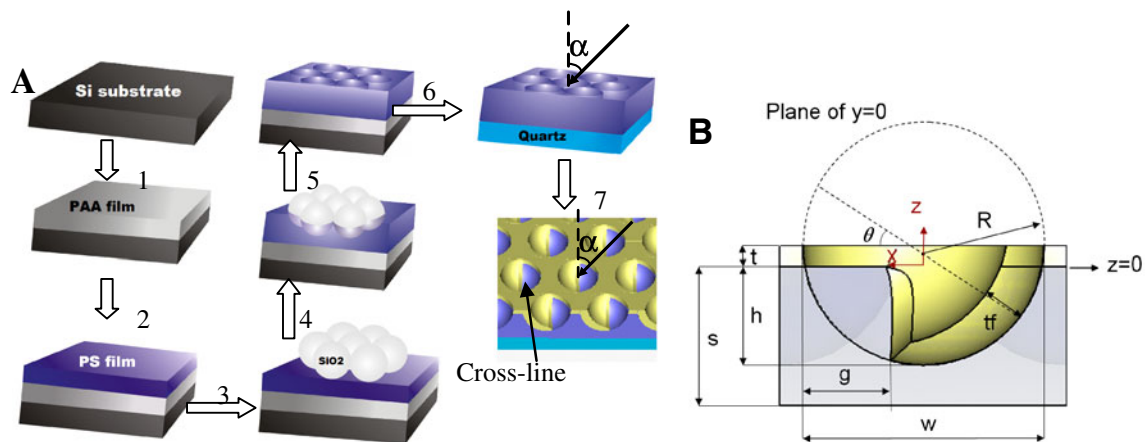


Fig. 1 **a** The fabrication procedure for a periodic array of three-dimensional crescent-like holes. 1 Spin-coating of sacrificial polyacrylic acid (PAA) film on silicon; 2 Spin-coating a layer of polystyrene (PS); 3 Spin-coating a multilayer of silica spheres with a diameter of 264 nm; 4 Heating the sample to let silica sphere embed into the PS film; 5 Removing the embedded silica particles by HF

solution; 6 The PAA film was dissolved in water, and a floating PS film with hemispherical dimple array was transferred to quartz slide; 7 A shadow metal evaporation method was employed to side deposit a layer of silver. **b** Cross-section view of the unit cell cutting along a line which passes through the center of the circle and perpendicular to the cross-line

lithography with shadow metal evaporation method. We report, to our knowledge, the first evidence of the extraordinary transmission induced by an asymmetric localized surface plasmon resonance in the arrays of 3DCLHs. This phenomenon can be useful for the coupling of the incident light to localized surface plasmon, e.g., for sensing applications. It is also valuable in the applications of sub-wavelength optoelectronic circuits.

Colloidal lithography has been widely exploited in the fabrication of surface plasmonic structures. By using two-dimensional array of colloidal spheres as templates, metal crescents, discs, holes, and split-ring resonators have been prepared after the various metal evaporation processes and reactive-ion etching procedure [30–34]. By utilizing thermal annealing to shape the interstitial holes of close-packed monolayer spheres, metal nano-ring, split-ring, and nano-disc can also be achieved without the reactive-ion etching process [35, 36]. Although colloidal nanospheres can directly form a template on the flat substrate, a large area of periodic monolayer spheres is usually hard to be achieved. Until recently, a method to introduce 2D nanostructure into the polymer film via colloidal lithography was reported [37, 38]. In this method, through thermal annealing or imprinting process, only the top or bottom layer of the spheres can be transferred to the polymer and form a large area of periodic array of monolayer spheres. It has been used to fabricate nano-metal shells, nano-dimples [37], nanograins [39], and nanodiscs [40]. Here, based on our previous work on fabricating nanodiscs [40], we have developed a method to prepare a periodic array of three-dimensional crescent-like holes.

Fabrication of 3D Crescent-like Holes Array

To fabricate 3D crescent-like holes array, an inverted hemispherical colloidal lithography method [40] is adopted; the fabrication procedure plotted in Fig. 1a can be described as follows: First, a layer of sacrificial polyacrylic acid (PAA) film was spin-coated on a cleaned silicon wafer, and baked at a hotplate with 120 °C for 5 min—the thickness of the PAA is around 220 nm; then, a layer of 137 nm polystyrene (PS) film was spin-coated on the sacrificial layer, the baking temperature and time were 120 °C and 5 min respectively; after that, the surface was modified by oxygen etching. Secondly, a multilayer of silica spheres with a diameter of 264 nm was spin-coated on the PS film, then the sample was placed on the hotplate with a temperature of 115 °C for 7 min to make the bottom layer of silica spheres embed into the PS film with a depth of around 98 nm. Thirdly, the silica spheres were removed by hydrofluoric acid (HF) with a concentration of 2%, a layer of dimple array was formed on the PS film, and then the PAA film was dissolved in water, a floating patterned PS film was formed and transferred onto the quartz slide. Finally, a shadow evaporation method was employed to deposit a layer of silver on the patterned PS film, a 3D crescent-like holes array was formed. The schematic structure of fabricated sample is shown in the last step of Fig. 1a. On the top surface, it looks like a periodic array of holes. However, within a unit cell, part of dimple is also deposited with silver because the shadow evaporation method can deposit metal on the part of the dimple by varying the deposition angle α , as shown in Fig. 1a. In other words, how much area within the dimple is deposited

with silver can be controlled by α . It looks like an array of crescent holes in top view; it is a three-dimensional structure. Here, it is named as a periodic array of three-dimensional crescent-like holes (3DCLH). The thicknesses of the silver at the top surface and the dimples are quite different since the metal evaporation angle varies at different parts within a unit cell. Figure 1b is the cross-sectional view of the unit cell by cutting along a line which passes through the center of the circle and is perpendicular to the cross-line. t is the thickness of the metal on the top of the PS film, θ is the metal evaporation angle, g is the gap width of the crescent-like hole, tf is the thickness of the thickest metal part where silver is deposited vertically. The interface between the PS top surface and metal layer is at $z=0$. The depth of the dimple before depositing metal layer is h . The diameter of the dimple is w .

Scanning electron microscope pictures of the samples are shown in Fig. 2. Figure 2a, b shows two periodic arrays of 3DCLHs, where black area is not covered with silver. The thicknesses of the silver at top plates in Fig. 2a and b are 55 and 37 nm, respectively. The diameter of the upper circles and the depth of the dimples before silver evaporation are about 255 and 98 nm, respectively. The period of the triangular structure is 283 nm. The area covered with silver is different for different samples. Here, we define f as a ratio of area without silver to the total area in the two-dimensional plane view. It should be noted that, due to the nature of colloidal lithography, the pattern is composed of many single domains in different orientations with maximum size of $10 \times 10 \mu\text{m}^2$.

Optical Measurement and Analysis

To characterize the optical properties of 3DCLHs, we measured the zero-order angle-resolved transmission for p-polarized waves (the electric field is on the incident plane). It should be pointed out that, in all the angle-resolved spectra shown in this paper, the curves are plotted with subsequent vertical offsets of 5% for each step increase of

incident angle. Figure 3a shows the results where the electric field is pointing along with the cross-line of the 3DCLH as shown in the inset. Two transmission dips are in 546 and 634 nm at normal incidence, as indicated by red arrows; these two dips are composed of a large dip. There are two peaks which are at 570 and 1,028 nm. In order to understand this transmission, we simulated the transmission of the 3DCLHs arrays via finite-difference time-domain (FDTD) method [41]. Because the domain size is about $10 \mu\text{m}$, the cross-lines of 3DCLHs are oriented to different direction from Γ - M to Γ - K in various domains with different lattice orientations. In simulation, we have to consider all these conditions. Here, we simulated various 3DCLHs arrays with their cross-lines oriented to different lattice directions, and made an average of these transmissions. The simulated transmission spectra of the 3DCLHs arrays with their cross-line parallel to Γ - M and Γ - K directions are nearly the same except that there is a surface plasmon polariton peak at 490 nm for Γ - M direction, as shown in Fig. 3b. This means that the different orientations of the crescent-like holes arrays have the same optical transmission when the wavelength is larger than 550 nm. In other words, when the wavelength is larger than 550 nm, the transmission property of the array are mainly decided by 3DCLH rather than the periodic structure. The simulation results show that there are two dips at 554 and 668 nm, and two peaks at 600 and 952 nm as well. Overall, the simulation results match with experimental results well, except that there exists a deviation at peak position which may be caused by the structure used in simulation not being perfectly the same as the real structure (the rough surface is not considered here). We further inspect the electric field distribution at each dips and peaks, as shown in Fig. 4a–d. It is found that, at the peak position of 962 nm, the electric field is concentrated on the outer surface of 3DCLH and strongly localized at the crescent tip, which enables the resonant field to be re-radiated into the PS film as transmitted wave. In a unit cell, the resonant mode is a dipole resonance, as indicated by the charge polarity. The strong localized field at the crescent tip is mainly caused by

Fig. 2 Scanning electron microscope pictures of 3DCLHs, where black area is not covered with silver. **a** 3DCLH with 55 nm thickness of silver at top plate; **b** 3DCLH with 37 nm thickness of silver at top plate

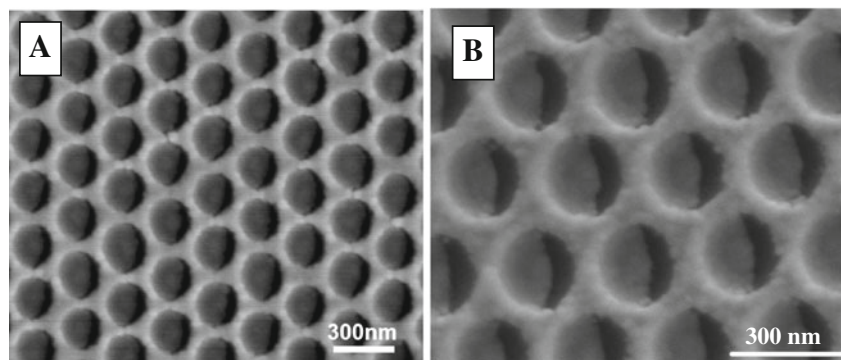
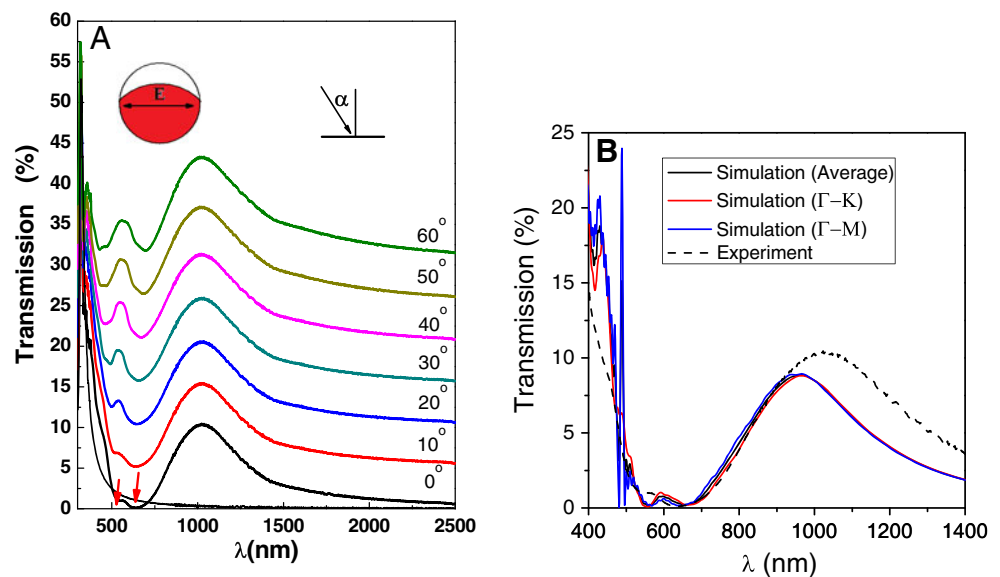


Fig. 3 a The zero-order angle-resolved transmission spectra of the 3DCLHs array shown in Fig. 2a for the electric field of incident p-polarized waves being along the cross-line; the curves have been plotted with subsequent vertical offsets of 5%. The black thin line is the transmission of a thin silver film with a thickness of 55 nm. The inserted red-white circles denote the electrical field of the incident beam, where red color indicates silver parts in the dimple, while white indicates the parts without silver. **b** The simulated and experimental transmission spectra in normal incidence



the crescent structure and rather than a periodic effect. At the dip position of 668 nm, the electric field is mainly trapped within the dimples covered with silver, and thus, most of which is reflected back into the air. Because the electric field is localized at the 3D crescent-like holes area, the peak at 962 nm and dip at 668 nm are caused by localized surface plasmon. This can also be found from the experimental angle-resolved transmission spectra of Fig. 3a, where the transmission peak position at 1,028 nm and dip position at 634 nm do not change with the change of incident angle. While for the peak position at 600 nm and dip position at 554 nm will change their positions with the change of the incident angle, this can be found from their electric field distribution which is weakly localized at dip's area, especially the area having silver. Their field distribu-

tions also indicate dipole resonance as well. This is caused by the combination of surface plasmon polariton and localized surface plasmon, the detailed mechanism becomes more complicated which requires further study.

Figure 5a represents the angle-resolved zero-order transmission when the electric field of the incident p-polarized waves is perpendicular to the cross-line of 3DCLH. Because the unit cell of the 3DCLHs array has no mirror symmetry for positive and negative incident angles, we measured the angle-resolved spectra from -60° to 60° as shown in the inset. There exists a wide dip at 595 nm when the incident angle is 0° . The peak transmission at normal incidence at the wavelength of 1,336 nm is about 32.22% which is much higher than that in the case of electric field being along with the cross-line

Fig. 4 The electric field amplitude at the plane of $z=-20$ nm when the cross-line of the 3DCLH oriented to $\Gamma-K$ for the electric field of the p-polarized waves parallel to the cross-line of the 3DCLH. **a** $\lambda=952$, **b** $\lambda=668$, **c** $\lambda=600$, and **d** $\lambda=554$ nm. The electric field amplitude distribution for the cross-line of the 3DCLH oriented to $\Gamma-M$ are nearly the same. The plus and minus signs indicate the polarity of the charge

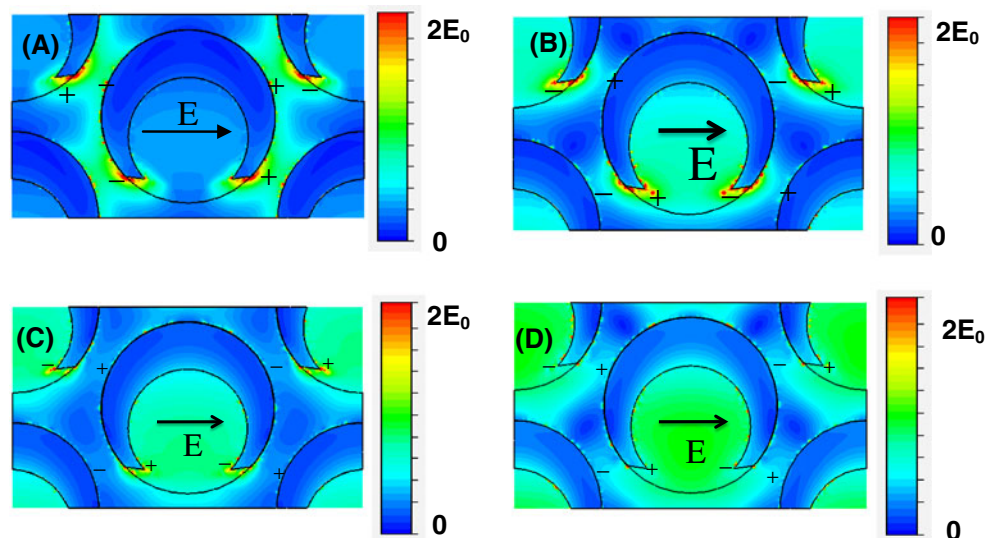
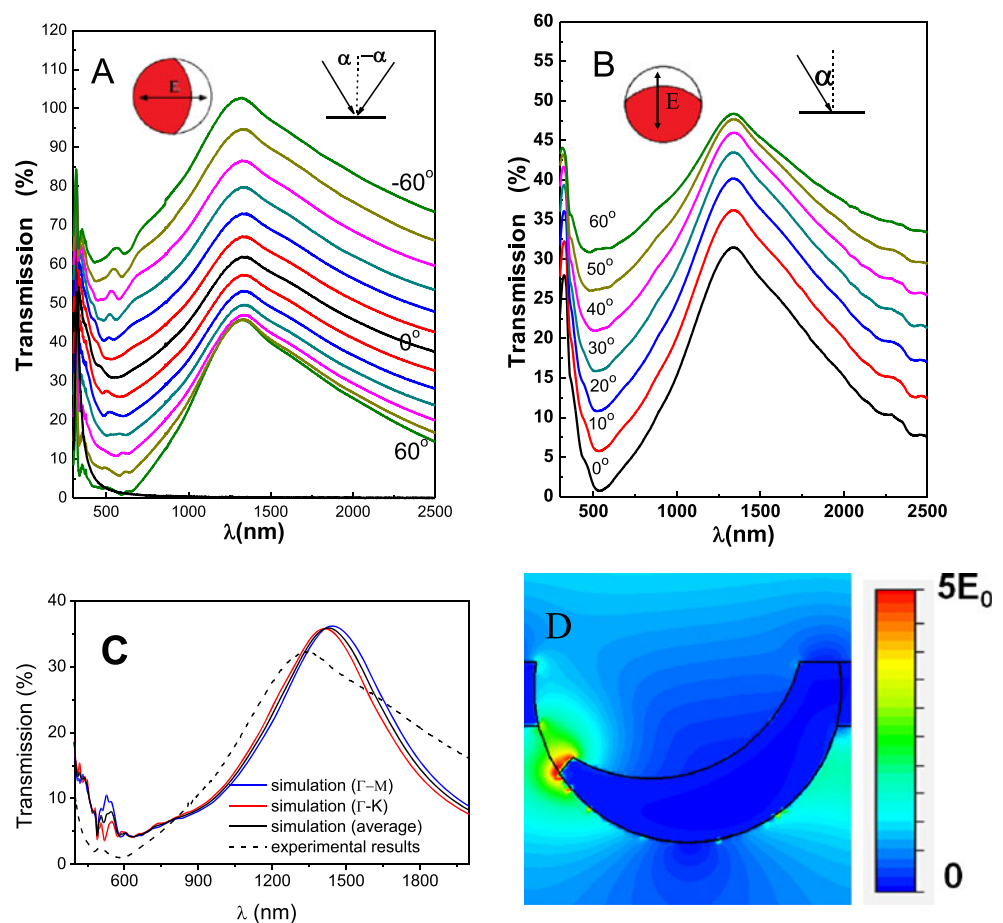


Fig. 5 **a** and **b** are the zero-order angle-resolved transmission spectra of the 3DCLHs array shown in Fig. 2a for the electric field being perpendicular to the cross-line of 3DCLH, **a** for p-polarized waves; **b** for s-polarized waves. In all spectra graphs, the curves have been plotted with subsequent vertical offsets of 5%. The *black thin line* in (**a**) is the transmission of a thin silver film with a thickness of 55 nm. The inserted *red–white circles* denote the electrical field of the incident beam, where *red color* indicates silver parts in the dimple, while *white* indicates the parts without silver. **c** The simulated and experimental transmission of 3DCLH's at normal incidence when the electric field is perpendicular to the cross-line of the 3DCLHs; **d** the electric field amplitude distribution at the wavelength of 1,442 nm in peak transmission at Fig. 5c



of 3DCLH. If the transmission is normalized with the fraction of holes' area of 7.7%, the transmission can be over 4.18, which exhibits an extraordinary optical transmission phenomenon. It is surprising that this transmission peak does not shift with the change of incident angle. To understand the physics of this transmission, we also simulate the transmission through FDTD method. It is shown in Fig. 5c, where the simulated transmission is an average of the transmissions of the 3DCLHs arrays when the cross-lines of 3DCLHs are oriented to Γ -M and Γ -K, respectively. The transmission spectra of the 3DCLHs arrays with different orientations of the 3DCLH's cross-line are shown in this figure. It is found that the transmission spectra of these two cases with different orientations of the cross-lines are nearly the same. This means that the orientation of the cross-line of the 3DCLH does not affect the transmission in the normal incidence. Comparing the simulating results with the experimental results, it is found that the shape of the transmission spectra agrees well with each other except that the position of the peak has slightly deviation where the simulating and experimental transmission peaks are at 1,442 and 1,336 nm, respectively. The deviation is caused by the simulation structure is not perfectly matching to the

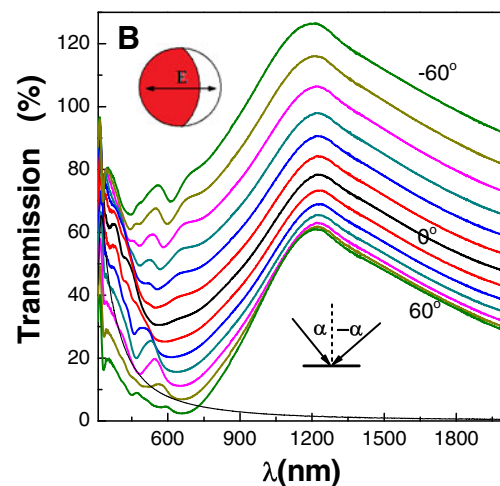


Fig. 6 The angle-resolved transmission spectra of the 3DCLHs array shown in Fig. 2b for the electric field of the incident p-polarized waves being vertical to the cross-line, where the *black thin line* is the transmission of a thin silver film with a thickness of 37 nm; the curves have been plotted with subsequent vertical offsets of 5%. The inserted *red–white circle* denotes the electrical field of the incident beam, where *red* indicates silver parts in the dimple, while *white* indicates the parts without silver

experimental one as mentioned before. For the wavelength shorter than 600 nm, it is not considered here because both SPP and LSP play roles in the transmission and makes it more complicated. Looking into the electric field distribution at the peak position shown in Fig. 5d, it can be found that the electric field is strongly localized at the low arc of the 3DCLH, which indicates an asymmetric localized surface plasmon resonance. Such a resonance, it could show an angle insensitive coupling to incident light similar to the symmetric localized plasmon resonance [27], this might be the reason why the peak is consistent with the change of the incident angle when the electric field of the incident beam is perpendicular to the cross-line of the 3DCLH. Therefore, we found a novel physical phenomenon of EOT whose peak position is determined by an asymmetric LSP rather than SPP. The peak position is nearly stable with the change of incident angles. It might be useful for the sub-wavelength integrated optics and optical sensors.

Because SPP can only exist efficiently in the p-polarized wave and does not exist in s-polarized waves [42] to further exclude the SPP effect on the abnormal EOT, we also measured the zero-order transmission when the electric field of the incident s-polarized waves is perpendicular to the cross-line of the 3DCLH, as shown in Fig. 5b. It is found that, even with the incident angle up to 60°, the transmission is still as high as 18.34%, and the peak position does not shift as well. Therefore, we could also obtain a conclusion that this EOT is induced by LSP rather than SPP.

To study this EOT in details, we fabricated various 3DCLHs arrays with different thicknesses of the silver film and various gaps. Figure 6 shows the p-polarized angle-resolved transmission of the 3DCLHs array with 37 nm thickness of silver as shown in Fig. 2b. The filling fraction of the crescent-like holes is 13.56%. For the electric field of the incident waves being perpendicular to the cross-line, there also exists an EOT peak (48.32%) at the wavelength of 1,228 nm which does not change with the incident angle, if it is normalized with the fraction of the holes' area, the transmission can reach 3.56. It is found that, if the hole area is nearly the same, the peak position shifts to the short wavelength with the increase of the thickness of the silver; if the thicknesses of the silver are nearly the same, the peak position shifts to the long wavelength with the decrease of the gap, and the normalized transmission with the fraction of the hole area is also becoming larger with the decrease of the gap.

Conclusion

In summary, we have developed a technique to fabricate periodic arrays of three-dimensional crescent-like holes

based on an inverted colloidal lithography method and shadow metal evaporation. The shape of 3DCLH can be adjusted via varying the evaporation angle. The optical measurements show that, there exists a shape-dependent EOT peak for the electric field of the incident beam perpendicular to the cross-line of the 3DCLH. Especially, this transmission peak position does not change with the incident angle, which is different from the previous reports. Experiments and simulations show that this EOT is dominated by an asymmetric localized surface plasmon resonance induced by 3DCLH. This might be valuable for the optical sensing and optical integrated circuits.

Acknowledgments Authors thank Prof. Che-Ting Chan and Prof. Zhao-Qing Zhang from Hong Kong University of Science and Technology with their fruitful discussion. This work is supported by the following projects: NNSFC (10774195, U0834001, 10974263, 10725420, and U0934002), Ministry of Education (grant 309024), Program for New Century Excellent Talents in University, and National Basic Research Program of China under grant no. 2010CB923200.

Open Access This article is distributed under the terms of the Creative Commons Attribution Noncommercial License which permits any noncommercial use, distribution, and reproduction in any medium, provided the original author(s) and source are credited.

References

1. Ebbesen TW, Lezec HJ, Ghaemi HF, Thio T, Wolff PA (1998) *Nature* 391:667
2. Genet C, Ebbesen TW (2007) *Nature* 445:39
3. DiMaio JR, Ballato J (2006) *Opt Express* 14:2380
4. Shinada S, Hashizume J, Koyama F (2003) *Appl Phys Lett* 83:836
5. Hashizume J, Koyama F (2004) *Appl Phys Lett* 84:3226
6. Guo BS, Song GF, Chen LH (2007) *Appl Phys Lett* 91:2
7. Garcia-Vidal FJ, Martin-Moreno L, Ebbesen TW, Kuipers L (2005) *Reviews of Modern Physics* 82:729
8. Dahlin A, Zach M, Rindzevicius T, Kall M, Sutherland DS, Hook F (2005) *J Am Chem Soc* 127:5043
9. Brolo AG, Gordon R, Leathem B, Kavanagh KL (2004) *Langmuir* 20:4813
10. Lesuffleur A, Kumar LKS, Brolo AG, Kavanagh KL, Gordon R (2007) *J Phys Chem C* 111:2347
11. Degiron A, Lezec HJ, Barnes WL, Ebbesen TW (2002) *Appl Phys Lett* 81:4327
12. Degiron A, Ebbesen TW (2005) *J Opt A-Pure Appl Opt* 7:S90
13. Koerkamp KJK, Enoch S, Segerink FB, van Hulst NF, Kuipers L (2004) *Phys Rev Lett* 92:18
14. Ruan ZC, Qiu M (2006) *Phys Rev Lett* 96:23
15. Liu HT, Lalanne P (2008) *Nature* 452:728
16. Gordon R, Brolo AG, McKinnon A, Rajora A, Leathem B, Kavanagh KL (2004) *Phys Rev Lett* 92:3
17. Garcia-Vidal FJ, Moreno E, Porto JA, Martin-Moreno L (2005) *Phys Rev Lett* 95:10
18. Orbons SM, Roberts A (2006) *Opt Express* 14:12623
19. Bao YJ, Peng RW, Shu DJ, Wang M, Lu X, Shao J, Lu W, Ming NB (2008) *Phys Rev Lett* 101:8

20. Wu S, Wang QJ, Yin XG, Li JQ, Zhu D, Liu SQ, Zhu YY (2008) *Appl Phys Lett* 93:101113
21. Wang C, Gu J, Han J, Xing Q, Tian Z, Liu F, Chai L, Li Y, Hu M, Wang Q (2010) *Appl Phys Lett* 96:251102
22. Mary A, Rodrigo SG, Martin-Moreno L, Garcia-Vidal FJ (2007) *Phys Rev B* 76:19
23. Zhan P, Wang ZL, Dong H, Sun J, Wu J, Wang HT, Zhu SN, Ming NB, Zi J (2006) *Adv Mater* 18:1612
24. Marani R, Marrocco V, Grande M, Morea G, D’Orazio A, Petruzzelli V (2011) *Plasmonics* 6:469
25. Hou Y (2011) *Plasmonics* 6:289
26. Rui G, Zhan Q, Ming H (2011) *Plasmonics* 6:521
27. Rodrigo SG, Mahboub O, Degiron A, Genet C, Garcia-Vidal FJ, Martin-Moreno L, Ebbesen TW (2010) *Opt Express* 18:23691
28. Yang JC, Gao HW, Suh JY, Zhou W, Lee MH, Odom TW (2010) *Nano Lett* 10:3173
29. Pang Y, Genet C, Ebbesen TW (2007) *Opt Commun* 280:10
30. Shumaker-Parry JS, Rochholz H, Kreiter M (2005) *Adv Mater* 17:2131
31. Zhu FQ, Fan DL, Zhu XC, Zhu JG, Cammarata RC, Chien CL (2004) *Adv Mater* 16:2155
32. Bukasov R, Shumaker-Parry JS (2007) *Nano Lett* 7:1113
33. Fredriksson H, Alaverdyan Y, Dmitriev A, Langhammer C, Sutherland DS, Zaech M, Kasemo B (2007) *Adv Mater* 19:4297
34. Prikulis J, Hanarp P, Olofsson L, Sutherland D, Kall M (2004) *Nano Lett* 4:1003
35. Kosiorsek A, Kandulski W, Glaczynska H, Giersig M (2005) *Small* 1:439
36. Hulteen JC, Van Duyne RP (1995) *J Vac Sci Technol A: Vac, Surf, Films* 13:1553
37. Jang SG, Choi DG, Heo CJ, Lee SY, Yang SM (2008) *Adv Mater* 20:4862
38. Chen ZM, Gang T, Yan X, Li X, Zhang JH, Wang YF, Chen X, Sun ZQ, Zhang K, Zhao B, Yang B (2006) *Adv Mater* 18:924
39. Heo CJ, Kim SH, Jang SG, Lee SY, Yang SM (2009) *Adv Mater* 21:1726
40. Xu HX, Rao WY, Meng J, Shen Y, Jin CJ, Wang XH (2009) *Nanotechnology* 20:46
41. Berenger JP (1996) *J Comput Phys* 127:363
42. Zayats AV, Smolyaninov II, Maradudin AA (2005) *Phys Rep* 408:131